Article

Effects of vinyltriethoxysilane and maleic anhydride grafted polypropylenes on the morphological, thermal, rheological and mechanical properties of polypropylene/clay nanocomposites

Heriarivelo Risite [1,*], Hicham Abou Oualid [2] , Khalil El Mabrouk[3]

[1] Département de Physique de l'Université de Toliara. Madagascar.; h.risite@gmail.com
[2] Faculty of Sciences and Technologies, Morocco; Hicham.abououalid@gmail.com
[3] INANOTECH, Rabat Design, Rue Mohamed El Jazouli, Madinat El Irfane 10100 Rabat, Morocco
* Correspondence: h.risite@gmail.com.

Academic Editor: name
Received: date; Accepted: date; Published: date

Abstract: The morphology and properties of polypropylene (PP) /organoclay nanocomposites prepared by melt processing were investigated with a special interest on the different effects of the use of different grafted PP as compatibilizers, i.e. maleic anhydride or silane-grafted species, PP-g-MA or PP-g-Si. When either PP-g-MA or PP-g-Si was added, better improvement of properties was achieved. The addition of PP-g-Si was found to increase the crystallization temperature upon the clay addition in comparison to PP-g-MA. Moreover, the PP-g-MA proved to be more efficient than PP-g-Si. The degree of reinforcement was found to be dependent on the interaction forces between the polymer matrix/clay, which resulted in intercalated/partial exfoliated structures for PP-g-Si while increasing clay content induced a change from exfoliated to intercalated using PP-g-MA, as revealed by transmission electron microscopy observations and X-ray diffraction analysis.

.

Keywords: Nanocomposites, Reinforcements, Polypropylene functionalization, Thermal properties, Mechanical properties, Rheology.

1. Introduction

Filler-reinforced polymeric nanocomposite systems with well-dispersed inorganic nanoparticles have a tendency to exhibit significant improvements in physical and mechanical properties over their neat resin counterpart. The most commonly produced nanocomposite systems are polymer-layered silicate nanocomposites, which are of interest because of their exceptional reinforcement effects at very low loading. This characteristic has been exploited to prepare commercially viable structural components since minimized nanofiller loading results in a lighter structure, good processability, and increased ductility [1].

Polypropylene (PP)/clay nanocomposites found many applications in industry. However, preparing well dispersed nanofiller in polymer matrix can pose a challenge during processing due to the difference in the polarity of nonpolar PP versus polar filler, which can lead to weak interfacial adhesion between polymer matrix and filler. To overcome this problem, a wide variety of polar groups such as maleic anhydride (MA), glycidyl methacrylate, acrylic acid, diethyl maleate, butyl acrylate, polyallyl have been used to achieve compatibilization and good dispersion, by grafting these molecules onto a polymer backbone [2–5]. This is expected to enhance the polarity of the PP, followed by the interfacial adhesion between polymer and filler.

Recently, vinylakoxysilanes such as vinyltrimethoxysilane (VTMS) and vinyltriethoxysilane (VTES) are used in manufacture of crosslinkable polyolefin. The two functional groups vinyl group and alkoxy can respectively be grafted on a PP backbone and be hydrolyzed to generate silanols that can be coupled with each other to form crosslinkage [6–13]. However, this technique may present problems on the final products because excess crosslinking loading could create defects at the shaping materials. In this regard, VTES grafted PP (PP-g-Si) was used and it was found that appropriate graft contents and the efficiencies of moisture-curing provided favorable rheological properties without attending the gel point [14]. It can thus be expected that the use of PP-g-Si as compatibilizer can cause an enhancement in the interaction between PP and clay with controlling the method of preparation.

The use of such molecules showed an improvement in the final properties of the resulting nanocomposites, however, the study of the degree of reinforcement of each molecule on one grade type of polymer (PP or polyethylene, PE) in the presence of the clay is not well documented. This would allow to assess the efficiency of each molecule compared to the other on a given polymer and permit to understand the parameters governing the property improvements. Contact angle measurement was used as a useful technique of measure of wettability for evaluation of compatibilizer species (i.e. isotactic homopolymer, MA grafted, and silane-grafted species) for the synthesis of a nanocomposite [15]. The maleated polymer and the organophilic coated clay were found to provide complete wetting, making the system an ideal candidate for subsequent intercalation. However, the experiments showing the difference in terms of properties have not been done.

Based on these points of view, in the present study, PP was functionalized by peroxide –initiated grafting of MA and VTES to obtain PP-g-MA and PP-g-Si derivatives respectively in order to prepare nanocomposites. The effects of the usage of the compatibilizers on the prepared nanocomposites were studied and assessed by X-ray diffraction (XRD), transmission electronic microscopy (TEM), thermogravimetric analysis (TGA), rheometry in small amplitude oscillatory shear and mechanical testing.

2. Results

2.1. Morphology and structural characterizations

Figure 2 showed a series of XRD patterns of all nanocomposites including virgin clay. C20A clay showed a peak centered at 2θ = 3.6°, corresponding to the basal plane peak d_{001} of 2.45 nm. For nanocomposites compatibilized with PP-g-Si, it was difficult to determine the interlayer spacing due to the peak broadening in comparison to the C20A peak. However, it should be noted that the peak characteristic of interlayer spacing was present at a small quantity, (around 2θ = 3.1°, corresponding to d_{001} of 2.94 nm). The decrease in intensity and the broadening of peak is probably due to the disorder generated by the stacks of layered silicates while maintaining a periodic distance and to the partial exfoliation of layered silicates. TEM observations of selected nanocomposites as shown in Figure 3 supported these assumptions. The microscopy confirmed that PP is intercalated into the interlayer spacing of clay galleries. In order to evaluate the d-spacing of intercalated PP-g-Si nanocomposites, the distance was also calculated within image J software and by using TEM images of intercalated PP/PP-g-Si/C20A3 recorded at higher magnifications (Figure 4). TEM observations were found to be in good concordance with XRD and the calculated interlayer spacing was found to be around 2.91 nm. However, using PP-g-MA, the interlayer characteristic peak appeared only at high clay loadings (8 wt%), which confirmed the complete exfoliated at clay loadings ≤5 wt% whereas coexistence of partial exfoliated and intercalated structures are obtained at 8 wt%. To explain this difference, the graft content and also the amplitude of polarity between VTES and MA are supposed to be responsible. In the case of PP-g-Si, and during melt extrusion, the alkylammonium-based clay has the same aliphatic apolar nature as the ethyl end groups of silane grafted onto the PP backbone (in another word, the silane grafted interacts with silicates via Van der Walls bonds, bonds of low energy) that induce the formation of stacked structure after cessation of shear. In the case of PP-g-MA, it was easier to create a hydrogen bonding with silicates (bonds of higher energy than Van der Walls bonds [17]), therefore, when equilibrium is reached, there is a sufficient excess enthalpy to promote an exfoliated nanocomposite structure. In fact, in the melt, the mass transport of the polymer, entering the interlayer space is fast, and the polymer chains exhibit a mobility similar or faster than the self-diffusion [18]. If thermodynamic conditions are favorable for intercalation, the polymer can crawl in and out of the interlayer space until equilibrium is reached

2.1. Thermal behaviour

Thermal stability

Figure 5 illustrates the TGA curves of virgin PP and nanocomposites based on silane and MA grafting PP. The detailed data corresponding to the decomposition temperatures at 5 % ($T_{5\%}$) and T_{max} are presented in Table 1. During thermal degradation, nanocomposites samples exhibited thermal decomposition temperature of about 5 to 14 °C at $T_{5\%}$ and from 43 to 58 °C at T_{max}, greater than degradation temperature of the matrix, for the nanocomposites prepared with PP-g-Si; whereas it was recorded a variation from 8 to 32 °C at $T_{5\%}$ and 89 to 98 °C at T_{max} greater than to that of the matrix for nanocomposites prepared with PP-g-MA. In comparison to the matrix, samples without clay exhibited a decrease in both $T_{5\%}$ and T_{max} with PP-g-Si as a compatibilizer and between $T_{5\%}$ and T_{max} for PP-g-MA. It was noted also that PP-g-Si samples stabilized gradually from 340 to 1000 °C with a residue of 5 to 2 wt%. Generally, the incorporation of clay into the polymer matrix enhances thermal stability by acting as a superior insulator and transport barrier to the volatile products generated during decomposition [19, 20]. The remarkable improvement in thermal stability of PP-g-MA clay nanocomposites may depend on the state of dispersion of clay into PP matrix and its content. The exfoliated structure of nanocomposites can easily lead to the char formation which limited the diffusion of the thermo-oxidation products during decomposition. At lower clay loading (3 wt%), even if complete exfoliation is obtained, the amount of clay is not enough to provide the char formation. However, at higher loading (5 wt%) of exfoliated nanocomposites, the highest thermal

decomposition temperature was observed (about 98 °C). When partial exfoliated structure was obtained, even if clay loading was high (case of 8 wt%), thermal decomposition temperature was reduced because partial exfoliation does not lead to stabilize materials despite the char formation. This would explain the differences observed between nanocomposites prepared with PP-g-MA and PP-g-Si.

Melting and crystallization properties.

Generally, the properties of semicrystalline thermoplastic materials are strongly related to their internal microstructure and crystallinity, particularly the mechanical properties and thermal stability [21]. Thermal parameters of crystallization (T_c) and melting (T_m) temperatures, crystallization enthalpy (ΔH_c), heat of melting (ΔH_m), and the percentage of crystallinity (X_c) are presented in Table 2. The crystallization thermograms of neat PP, PP/PP-g-Si and PP/PP-g-MA blends and nanocomposites are shown in Figure 6(a). The results showed the differences between nanocomposites compatibilized with PP-g-Si and nanocomposites based on PP-g-MA. For neat PP, the crystallization temperature (T_c) was observed at around 114.79 °C. Furthermore, for PP/PP-g-Si blend, T_c increased by about 8 °C, while PP/PP-g-MA showed no significant increase. In addition, the nanocomposites based on PP-g-Si presented a remarkable increase of T_c in comparison to those prepared with PP-g-MA (of about 17 ºC for 8 wt% of clay content). In the case of PP-g-MA, only the intercalated composition (with 8 wt% of clay) recorded an enhancement in crystallization temperature. This increase is informative of a heterogeneous nucleation process in the presence of clay, which induced and facilitated the crystallization process of PP during cooling and thus promoted by the presence of PP-g-Si which act as a nucleating agent during PP crystallization. This is also observed by the increase of crystallinity content of nanocomposites prepared with PP-g-Si upon clay addition and the decrease for PP-g-MA nanocomposites (Table 2). From Figure 6(b), neat PP exhibited a melting temperature at around 165.34 °C and the binary blends and all nanocomposites showed a slight shift up to 3 °C in the melting point (Table 2). In summary, the differences in the crystallization characteristics of PP by the addition of clays are of crucial importance for understanding the mechanical properties of prepared nanocomposites.

2.1. Morphological properties

Linear viscoelastic properties are helpful in determining the strength of polymer layered silicate interactions and the structure-property relationship in nanocomposites at low frequencies range [22]. Figure 7 presents the storage modulus G' and complex viscosity η* as function of frequency for PP, PP-g-Si, PP-g-MA, PP/PP-g-Si, PP/PP-g-MA and corresponding nanocomposites obtained with different clay loadings. Compared to PP, both modified PP showed lower complex viscosity. At low frequencies, reduced melt viscosity of PP-g-Si was pronounced whereas the presence of PP-g-MA was found to be changed slightly. When clay content was increased, a dramatic rise was noted in both of G' and η*, leading to the plateau in the shear moduli and non-Newtonian behavior viscosity, for nanocomposites compatibilized with PP-g-MA, at low frequencies. For nanocomposites compatibilized with PP-g-Si, storage modulus and complex viscosity behaviors were identical to those of the neat PP and increased progressively with the increase of clay content, keeping Newtonian behavior in viscosity. These noticeable differences were namely related to the difference in the state of dispersion of clay and to the interaction between components. In the presence of PP-g-Si, alkylammonium surfactant/polymer interaction was favored which lead to intercalated/partial exfoliation since the silane end group grafted onto PP is ethyl, and polymer interacts with clay by Van der Waals interaction, promoting silicates interactions. However, MA grafted onto PP is capable

of hydrogen bonding with hydroxyl group of clay lamella leading to better dispersion of those clay lamellas in matrix, as revealed by TEM observations and XRD analysis. It is noteworthy to mention that the bond energy of hydrogen bonds is lower than covalent bonds but much higher than the bond energy of Van der Waals forces between two atoms. Consequently, when the clay content is increased, the extent of percolated network structures formed by exfoliated layers or stacks of intercalated layers also called tactoids increased [23]. When subjected to shear, individual lamellae and tactoids are beyond a critical volume fraction, incapable of rotating freely and thus prevented from complete relaxation [24].

2.1. Tensile properties

Homogeneous dispersion of clay nanolayers in polymer matrix is known to provide reinforcement via load transfer and deflection of cracks resulting from an applied load, due to its high aspect ratio and platelet structure. Interactions between exfoliated nanolayers with wide interfacial area and the surrounding polymer matrix can lead to higher mechanical properties [25]. The tensile properties of samples were determined to establish the effect of compatibilizing agents and the clay content. Figure 8 shows the Young's modulus of PP, PP-g-Si, PP-g-MA, PP/PP-g-Si, PP/PP-g-MA and nanocomposites obtained with different clay contents. It can be seen from the results that all nanocomposites achieved higher modulus than neat PP, while as expected PP-g-Si and PP-g-MA decreased. This reduction is attributed to the chain scission resulting from chemical treatment of PP with peroxides, lowering PP molecular weight and consequently the mechanical properties. Clear differences in the tensile properties of the nanocomposites with different type of compatibilizer are shown. The property enhancements of nanocomposites became more significant with the incorporation of the PP-g-MA compared to PP-g-Si compatibilizer. As mentioned above, the state of dispersion, the level of interaction strength between the organoclay and polymer and the rheological properties of nanocomposites containing PP-g-MA were much enhanced compared to compositions based on PP-g-Si.

2.2. Figures, Tables and Schemes

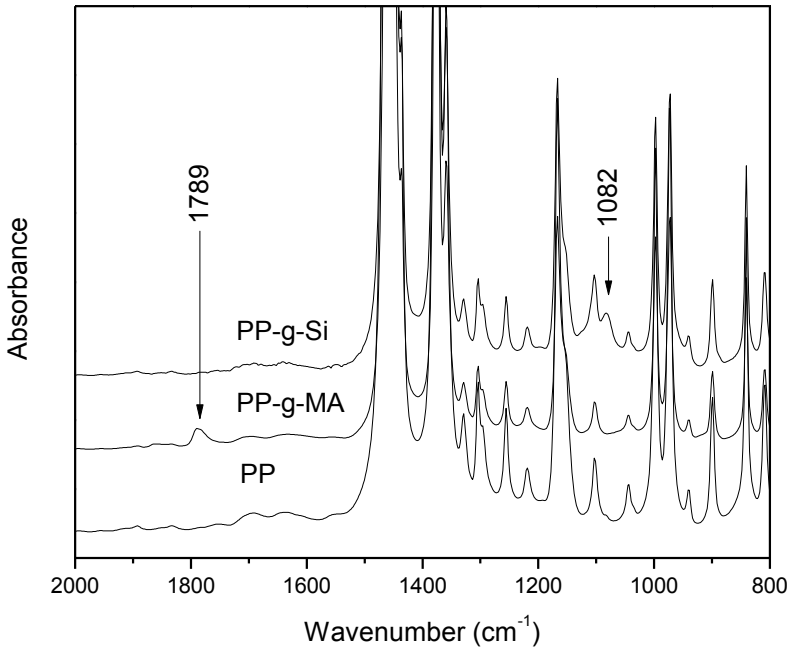

188

189 **Figure 1.** FTIR spectra of PP, PP-g-Si and PP-g-MA

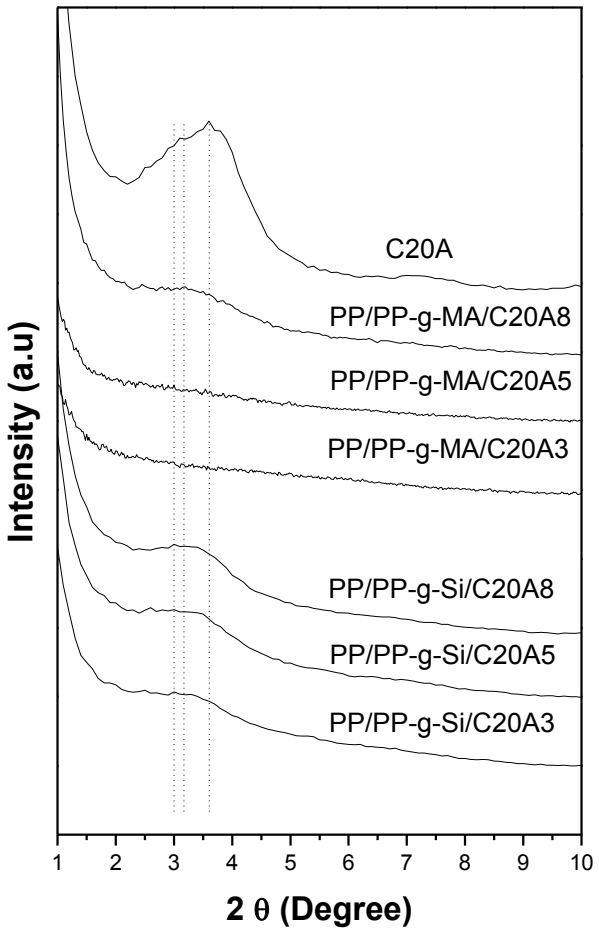

190

191 **Figure 2.** XRD patterns for the clays and PP nanocomposites at different clay contents

192

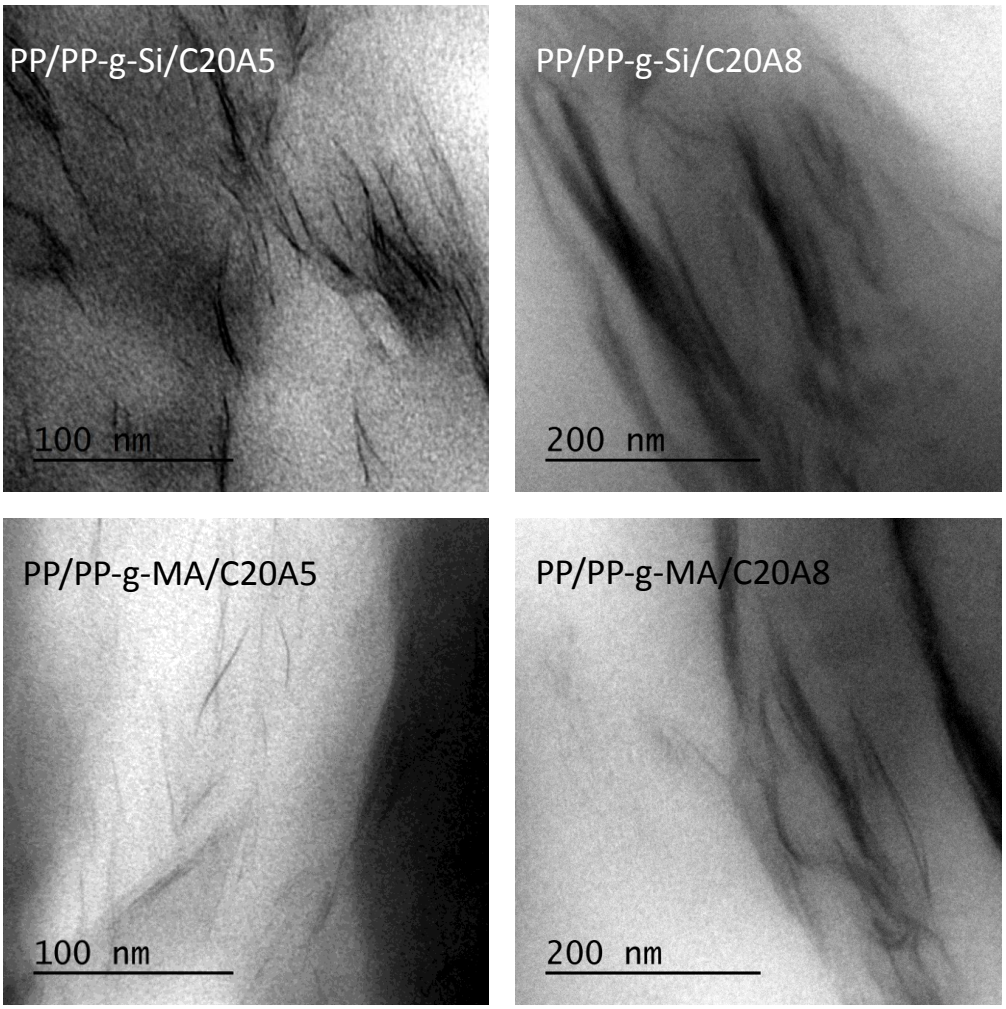

193

194 **Figure 3.** TEM micrographs of nanocomposites at 5 and 8 wt% clay contents

195

196

197

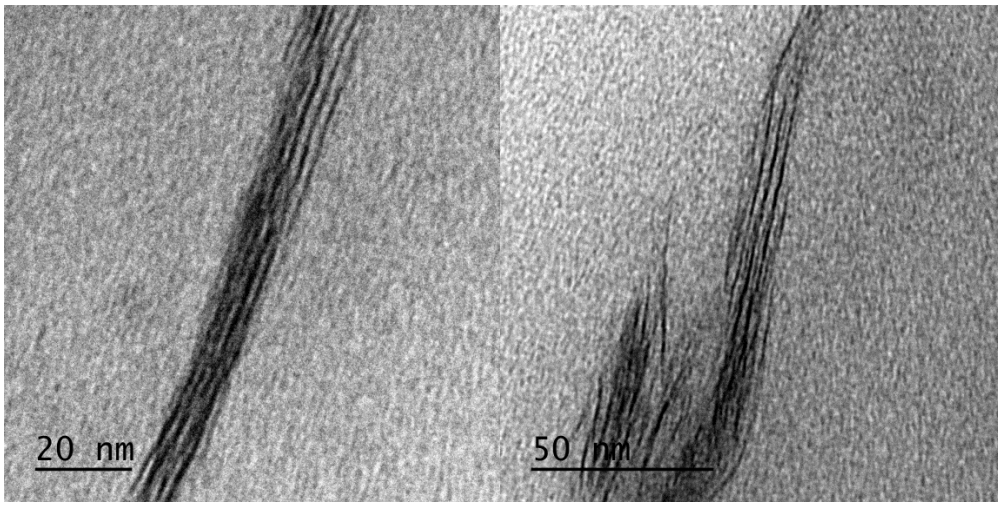

198

Figure 4. TEM micrographs of intercalated parts of PP/PP-g-Si/C20A3 nanocomposite

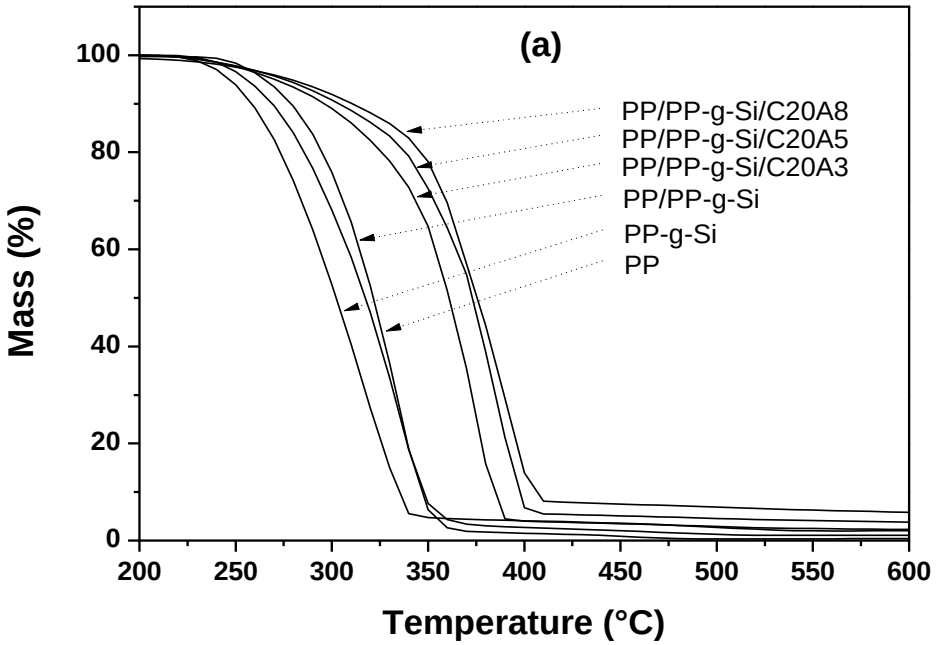

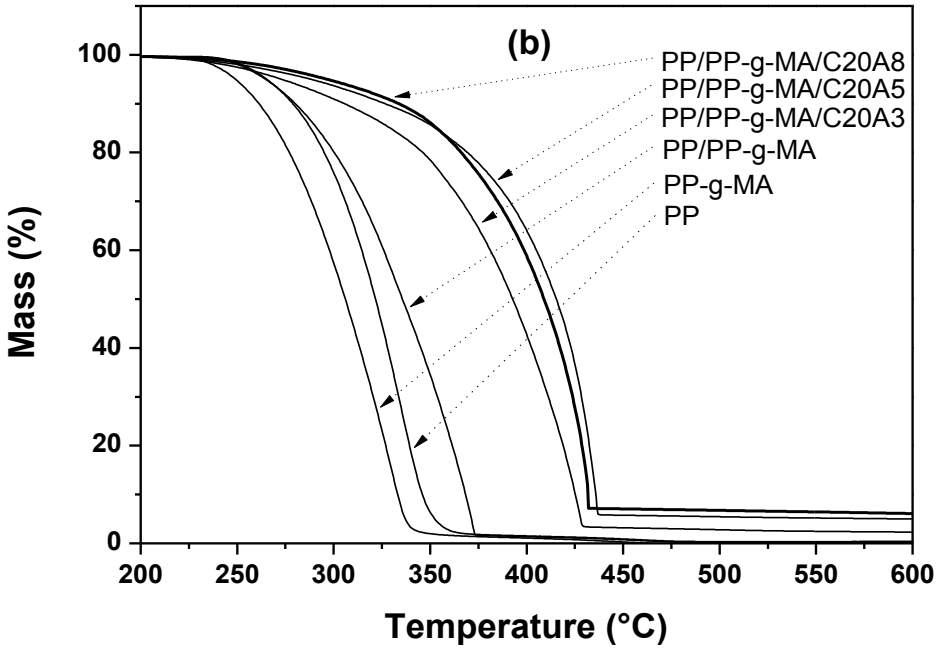

Figure 5. TGA curves of pure PP, PP-g-Si, PP-g-MA, PP/PP-g-Si, PP/PP-g-MA and all nanocomposites at different clay contents

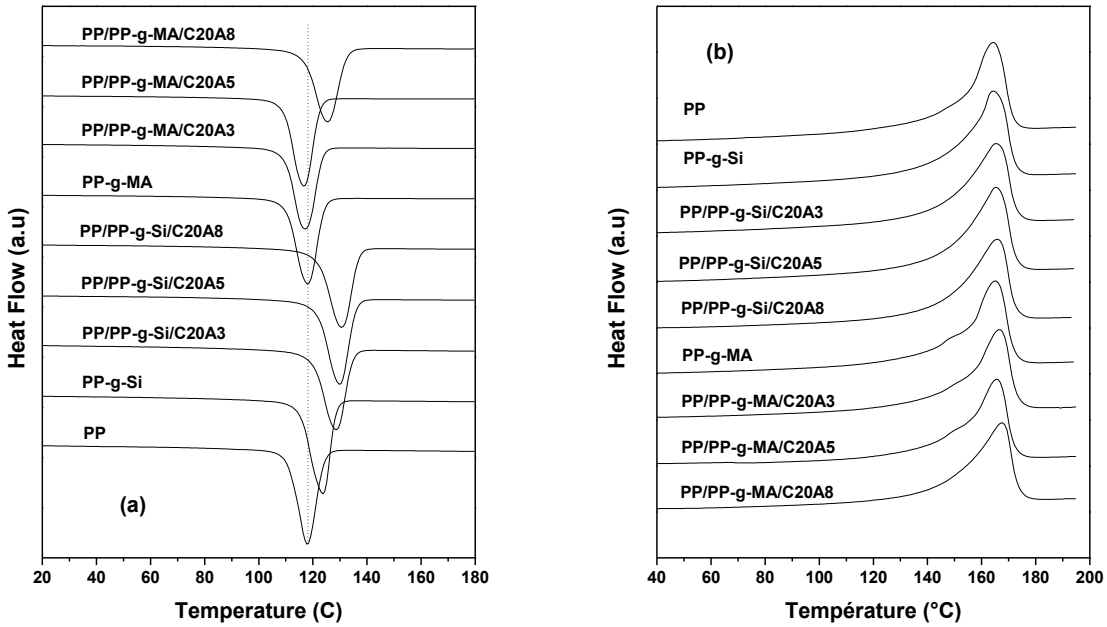

205 **Figure 6.** Crystallization thermograms (first cooling cycle) (a) and melting thermograms (second heating cycle)

206 (b) of neat PP and its nanocomposites with various clay contents at 10 °C/min cooling and heating rates

207

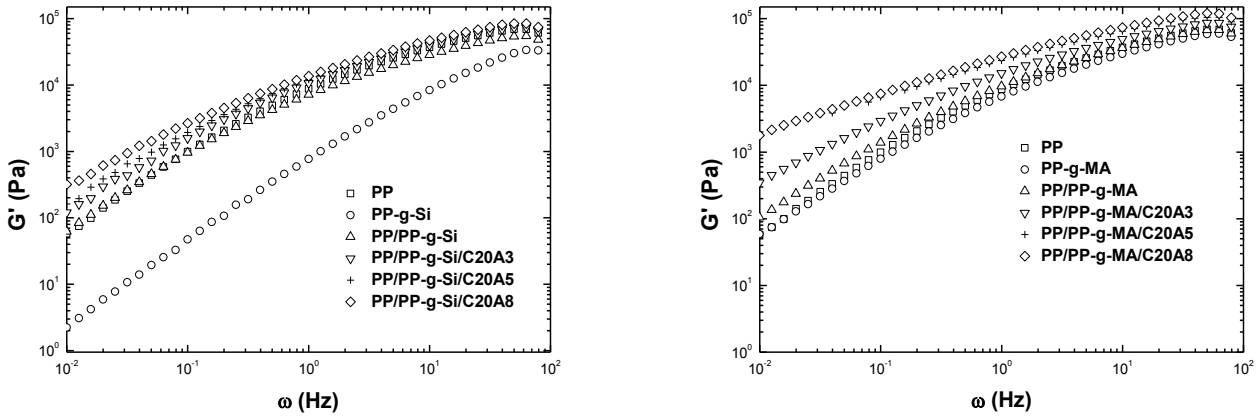

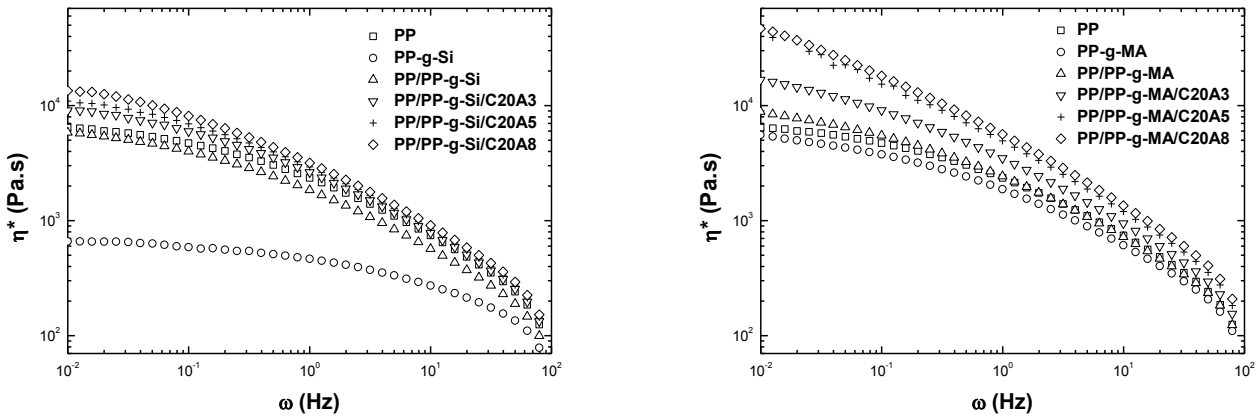

208 **Figure 7.** Elastic modulus G′ and complex viscosity η* at 180 °C as a function of the frequency of pure PP, PP-

209 g-Si, PP-g-MA, PP/PP-g-Si, PP/PP-g-MA and all nanocomposites at different clay contents

210

211

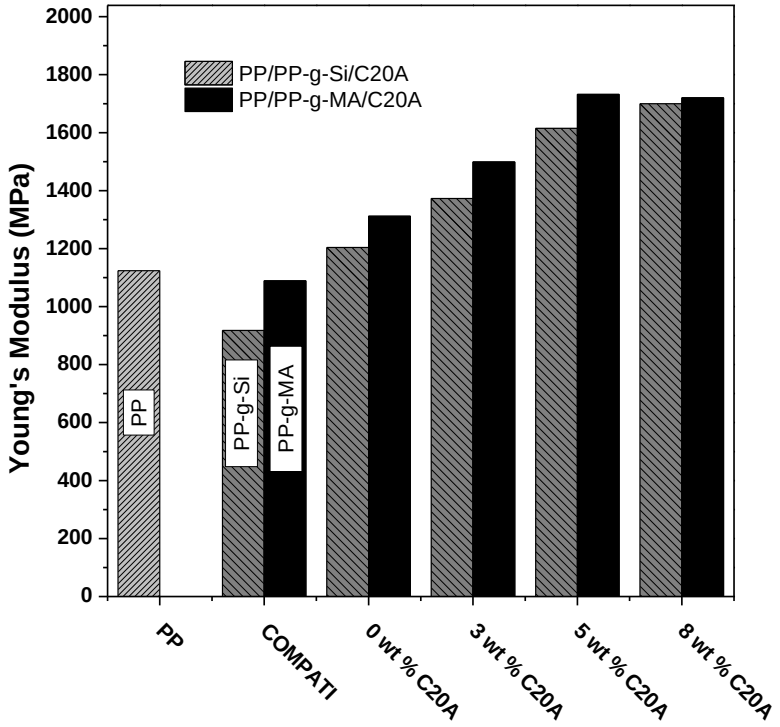

212

213 **Figure 8.** Mechanical properties of pure PP and their corresponding nanocomposites at different clay contents.

214 **Table 1.** TGA data of pure PP, PP-g-Si, PP-g-MA, PP/PP-g-Si, PP/PP-g-MA and all nanocomposites at different

215 clay loadings

Sample	$T_{5\%}$ (°C)	Improvement (°C)	T_{max} (°C)	Improvement (°C)
PP	265	reference	334	reference
PP-g-Si	247	-18	316	-18
PP/PP-g-Si	256	-9	333	-1
PP/PP-g-Si/C20A3	270	5	377	43
PP/PP-g-Si/C20A5	275	10	384	50
PP/PP-g-Si/C20A8	279	14	392	58
PP-g-MA	249	-16	327	-7
PP/PP-g-MA	265	0	350	16
PP/PP-g-MA/C20A3	273	8	423	89
PP/PP-g-MA/C20A5	288	23	432	98
PP/PP-g-MA/C20A8	297	35	427	93

216 **Table 2.** Summarized results of DSC analysis of PP and its nanocomposites with different clay content

	T_c (°C)	ΔH_c (J/g)	T_m (°C)	ΔH_m (J/g)	X_c (%)

PP	114.79	105.18	165.34	105.66	50.50
PP/PP-g-Si	122.31	108.84	165.34	108.66	51.92
PP/PP-g-MA	115.70	106.20	166.91	104.46	49.93
PP/PP-g-Si/C20A3	127.25	103.20	167.01	105.60	52.03
PP/PP-g-Si/C20A5	128.09	105.30	167.00	109.26	54.97
PP/PP-g-Si/C20A8	131.08	102.36	168.60	104.82	54.46
PP/PP-g-MA/C20A3	114.75	102.54	166.99	99.66	49.11
PP/PP-g-MA/C20A5	114.89	101.58	166.12	97.62	49.14
PP/PP-g-MA/C20A8	123.92	99.48	168.56	100.56	51.68

3. Discussion

4.Materials and Methods

Materials

The PP used throughout this investigation was a homopolymer, PP 5032E1, commercialized by Exxon Mobil chemical. Dicumyl peroxide (DCP, 98 %), vinyltriethoxysilane (VTES, 97 %) and maleic anhydride (MA, 99 %) were purchased from Sigma Aldrich. The filler were layered silicate, chemically modified with a dimethyl, dehydrogenated tallow quaternary ammonium salt (Cloisite 20A, C20A) purchased from southern Clay products Inc.

Grafting procedure

PP-g-Si. PP powder (50g) was tumble mixed with a solution of DCP (0.2 wt%) in VTES (5 wt%) for 20 min. The grafting reaction was carried out in Haake Polylab rheometer equipped with Rheomix mixing chamber and roller rotor. The mixture was reacted for 5min at 180 °C at a rotation speed of 60 rpm, giving PP-g-Si.

PP-g-MA. PP powder (50 g) was tumble mixed with a solution of chloroform and DCP (0.2 wt%) in MA (5 wt%) for 20 min. The grafting reaction was carried out in the same condition as PP-g-Si. The mixture is denoted as PP-g-MA

Nanocomposites preparation

Melt mixing of PP/PP-g-Si (or PP-g-MA)/C20A composites were carried out using contra-rotating twin screw micro extruder Minilab II. PP, PP-g-Si (or PP-g-MA) and clay were tumble mixed and introduced in the hopper. 500 ppm of irganox-1010, 1000 ppm of Irgafos-168 and 600 ppm of calcium stearate were added after 5 min of mixing time for 2 min to stabilize the PP-g-Si for nanocomposites samples. The temperature, screw speed and residence time were fixed at 180 °C, 60 rpm and 5 min respectively. The composition of PP/PP-g-Si (or PP-g-MA) is kept at 90 and 10 wt% for all blends and the clay concentrations were fixed at 3, 5 and 8 wt%. The notation used in the following for defining the blend composition is PP/PP-g-Si/ (or PP-g-MA)/C20A, and is expressed in weight fraction.

Characterizations and techniques

Characterization of functionalized PP.

PP-g-Si samples for graft content analysis were purified form residual VTES by dissolving in hot refluxing xylene stabilized in 100 ppm of 2,6-di-t-butyl-4-methylphenol (BHT), precipitating from acetone and dried under vacuum at 60 °C. FTIR spectra were obtained using an ABB Bomem FTLA

2000-102 FTIR instrument, in transmission mode (Figure 1). Grafted VTES contents were calculated from FTIR integrations of the 1064-1094 cm^{-1} absorbance of the silane relative to 422-496 cm^{-1} internal standard region originating from PP. A calibration curve for determining the graft content was obtained by using known mixtures of PP and unreactive silane as standards. Based on the calculation the grafted VTES content was determined to be 0.51 wt%.

PP-g-MA samples were purified from residual MA by dissolving in hot refluxing xylene, precipitating from acetone, and dried under vacuum at 60 °C. Grafted MA contents were calculated from FTIR integrations of the area derived from 1754-1808 cm^{-1} C=O anhydride absorbance relative to a 422-496 cm^{-1} internal standard region originating from PP. Calibration standards for this FTIR method were prepared by melt mixing known quantities of 1-dodecenylsuccinic anhydride to purified starting material. The grafted MA content was determined to be 0.33 wt%.

Morphology studies.

The structure of layered silicates and the morphology of composites were analyzed by X-ray scattering, Bruker D8 AXS X-ray diffractometer. Diffraction spectra were obtained over a 2θ range of 1-10° and the interlayer spacing (d_{001}) is calculated using the Bragg equation: $n\lambda=2d_{hkl}\sin\theta$, where λ is the wavelength of radiation (Cu-Kα radiation of 1.542 Å). The samples were prepared as discs of 25 mm in diameter and 1.5 mm in thickness, by compression molding at 180 °C. Each measurement was repeated four times, on two different surfaces. TEM observations were performed with a Philips CM200 TEM microscope operating at 200 kV and coupled to an energy dispersive (EDS) microprobe analyzer (EDAX DX-4). Ultrathin sections (ca. 100 nm) were cut into pieces with an ultramicrotome (Leica EM UC7) using a diamond knife at room temperature. The pieces were put on a carbon-coated copper TEM grid and then imaged with a TEM apparatus.

Thermal properties (TGA and DSC).

Thermogravimetric analyses (TGA) were conducted by using a Q500 TA instrument thermoanalyzer. The specimens with weights of about 15 mg were heated from room temperature to 1000 °C at a linear heating rate of 10 °C/min. All runs were performed in an air atmosphere at a flow of 60 ml/min.

The melting and crystallization behaviors of samples (approximately 12 mg) were analyzed by the usage of the conventional differential scanning calorimeter DSC-Q100 from TA Instrument. The heating program was as follows:

- first heating scan: Heating from 25 to 200 °C with a rate of 10 °C/min,
- keeping the sample at 200°C for 5 min to erase the thermal history.
- first cooling scan: cooling to -60 °C with a rate of 10 °C/min,
- second heating scan: Heating from -60 to 200 °C with a rate of 10°C/min.

All DSC runs were carried out under nitrogen atmosphere. The melting and crystallization peaks were obtained from the second heating and first cooling scans, respectively. The degree of crystallinity (X_c) was determined by using the following equation:

$$X_c(\%) = \frac{\Delta H_m}{(1-\phi)\Delta H_m^0} \times 100 \quad (1)$$

where ϕ was the clay content, ΔH_m was the apparent melting enthalpy, ΔH_m^0 was the extrapolated value of the enthalpy corresponding to the melting of 100% crystalline PP (ΔH_m^0 = 209.2 J/g [16])

Rheological measurements.

Rheological characterizations were performed in small-amplitude oscillatory shear flow on an ARES-LS rheometer, using parallel plate geometry with 25 mm in diameter and 1 mm in gap. Test specimens were prepared by compression molding at 180 °C. The storage and loss moduli, G′ and *G*′′, and complex shear viscosity, η^*, were measured over a frequency (ω) range of 0.01-100 Hz at 180 °C. All measurements were carried out in the liner viscoelastic regime by imposing a strain of 0.05 % as assessed by preliminary strain sweep tests.

Mechanical properties. Specimens for mechanical testing were prepared by compression molding at 180 °C using a carver press. Tensile properties were measured using an Instron 8810S universal tester machine, according to ASTM D638, at crosshead speeds of 10 mm/min. At least 5 specimens were tested for each sample and average values were reported here.

5. Conclusions

PP/clay nanocomposites based on PP-g-Si and PP-g-MA as compatibilizing agents were prepared by melt compounding. The presence of compatibilizers impacted the interaction polymer/filler, inducing therefore the morphology change during processing of nanocomposites. The use of PP-g-Si leaded to partial exfoliated/intercalated structures whereas PP-g-MA resulted in exfoliated structure at lower clay contents (≤ 5 wt%) and coexistence of exfoliated and intercalated structure at 8 wt%. The improvement in properties is related to the polymer-clay characteristics, the level of interaction between clay and polymer, and the obtained morphology. From thermal analysis, the presence of PP-g-Si induced an increase in crystallization temperature and crystallinity of nanocomposites upon clay addition in comparison to PP-g-MA. An increase in thermal stability was also observed in both compatibilized nanocomposites. Higher value (98 °C) was obtained in 5 wt% of clay with PP-g-MA. The increase of clay content significantly changed the rheological behavior of nanocomposites at low frequency regions, reaching a pseudo-solid like behavior. Rheological measurement also informed about the state of clay dispersion in polymer matrix. Significant mechanical reinforcement was also obtained and PP-g-MA showed better Young's modulus.

Acknowledgments: This work was funded by MAScIR - Moroccan Foundation for Advanced Science, Innovation and Research. The support from Hassan II Academy of Science and Technology, Rabat, Morocco is also greatly appreciated. The authors are grateful for the financial support from EC (project REGPOT AL-NANOFUNC grant number REGPOTCT-2011-285895-Al-NANOFUNC – FP7)

Author Contributions: "Risite conceived and designed the experiments; Risite performed the experiments; Risite. and Khalil El Mabrouk. analyzed the data; Khalil El Mabrouk. contributed reagents/materials/analysis tools; Risite. wrote the paper. Hicham Abou oualid improve the discussion and edit the paper."

Conflicts of Interest: We declare that this manuscript is original, has not been reported before, and is not currently being considered elsewhere. We also confirm that there is no known conflict of interest regarding this manuscript and its publication. The manuscript has been approved by all named authors.

References

1. Sinha Ray S and Okamoto M. Polymer/layered silicate nanocomposites: a review from preparation to processing. *Prog Polym Sci* 2003; 28: 1539–1641.
2. Lertwimolnun W and Vergnes B. Influence of compatibilizer and processing conditions on the dispersion of nanoclay in a polypropylene matrix. *Polymer* 2005; 46: 3462–3471.
3. Ding C, Jia D, He H, Guo B and Hong H. How organo-montmorillonite truly affects the structure and properties of polypropylene. *Polym Test* 2005; 24: 94–100.
4. López-Quintanilla ML, Sánchez-Valdés S, Ramos de Valle LF and Medellín-Rodríguez FJ. Effect of some compatibilizing agents on clay dispersion of polypropylene-clay nanocomposites. *J Appl Polym Sci* 2006; 100: 4748–4756.
5. Sengupta SS, Parent JS and McLean JK. Radical-mediated modification of polypropylene: Selective grafting via polyallyl coagents. *J Polym Sci Part A Polym Chem* 2005; 43: 4882–4893.
6. Bailly M and Kontopoulou M. Preparation and characterization of thermoplastic olefin/nanosilica composites using a silane-grafted polypropylene matrix. *Polymer* 2009; 50: 2472–2480.
7. Lu H, Hu Y, Li M, Chen Z and Fan W. Structure characteristics and thermal properties of silane-grafted-polyethylene/clay nanocomposite prepared by reactive extrusion. *Compos Sci Technol* 2006; 66: 3035–3039.
8. Sánchez-Valdes S, Méndez-Nonell J, Medellín-Rodríguez FJ, Ramírez-Vargas E, Martínez-Colunga JG, Soto-Valdez H, et al. Effect of PEgMA/amine silane compatibilizer on clay dispersion of polyethylene-clay nanocomposites. *Polym Bull* 2009; 63: 921–933.
9. Dal Castel C, Pelegrini T, Barbosa RV, Liberman SA and Mauler RS. Properties of silane grafted polypropylene/montmorillonite nanocomposites. *Compos Part A Appl Sci Manuf* 2010; 41: 185–191.
10. Liaw W-C, Huang P-C, Chen C-S, Lo C-L and Chang J-L. PPgMA/APTS compound coupling compatabilizer in PP/clay hybrid nanocomposite. *J Appl Polym Sci* 2008; 109: 1871–1880.
11. Russell KE. Free radical graft polymerization and copolymerization at higher temperatures. *Prog Polym Sci* 2002; 27: 1007–1038.
12. Santos KS, Liberman SA, Oviedo MAS and Mauler RS. Polyolefin-based nanocomposites: the effect of organosilane on organoclay dispersion. *J Mater Sci* 2013; 49: 70–78.
13. Nachtigall SMB, Stedile FC, Felix AHO and Mauler RS. Polypropylene Functionalization with Vinyltriethoxysilane. *Jounal Appl Polym Sci* 1998;72:1313–1319.
14. El Mabrouk K, Parent JS, Chaudhary BI and Cong R. Chemical modification of PP architecture: Strategies for introducing long-chain branching. *Polymer* 2009; 50: 5390–5397.
15. Rogers K, Takacs E and Thompson MR. Contact angle measurement of select compatibilizers for polymer-silicate layer nanocomposites. *Polym Test* 2005; 24: 423–427.
16. Chow WS, Mohd Ishak ZA, Karger-Kocsis J, Apostolov AA and Ishiaku US. Compatibilizing effect of maleated polypropylene on the mechanical properties and morphology of injection molded polyamide 6/polypropylene/organoclay nanocomposites. *Polymer* 2003; 44: 7427–7440.
17. Wiederrecht GP. *Handbook of nanofabrication*. Amsterdam; Boston: Elsevier; 2010.
18. Giannelis EP, Krishnamoorti R and Manias E. Polymer-Silicate Nanocomposites : Model Systems for Confined Polymers and Polymer Brushes. *Advances in Polymer Science* 1999; 138: 107–147.
19. Devalckenaere M, Je R, Dubois P and Kubies D. Poly (1 -caprolactone)/ clay nanocomposites prepared by melt intercalation : mechanical , thermal and rheological properties. *Polymer* 2002; 43: 4017–4023.

374 20. Zhu J, Morgan AB, Lamelas FJ and Wilkie CA. Fire Properties of Polystyrene - Clay Nanocomposites.
375 *Chem Mater* 2001; 13: 3774–3780.
376 21. Bureau MN, Denault J, Cole KC and Enright GD. The role of crystallinity and reinforcement in the
377 mechanical behavior of polyamide-6/clay nanocomposites. *Polym Eng Sci* 2002; 42: 1897–1906.
378 22. Ray SS. Rheology of Polymer / Layered Silicate Nanocomposites. *J Ind Eng Chem* 2006; 12: 811–842.
379 23. Kim DH, Fasulo PD, Rodgers WR and Paul DR. Structure and properties of polypropylene-based
380 nanocomposites: Effect of PP-g-MA to organoclay ratio. *Polymer* 2007; 48: 5308–5323.
381 24. Hyun YH, Lim ST, Choi HJ and Jhon MS. Rheology of Poly(ethylene oxide)/Organoclay
382 Nanocomposites. *Macromolecules* 2001; 34: 8084–8093.
383 25. Liang J-Z. Toughening and reinforcing in rigid inorganic particulate filled poly(propylene): A review. *J*
384 *Appl Polym Sci* 2002; 83: 1547–1555.
385